Supporting Information Appendix

Non-equilibrium Dynamics of Helix Reorganization Observed by Transient 2D IR Spectroscopy

Matthew J. Tucker, Mohannad Abdo, Joel R. Courter, Jianxin Chen, Stephen P. Brown, Amos B. Smith, III,* and Robin M. Hochstrasser*,#

Department of Chemistry, University of Pennsylvania, Philadelphia, PA 19104-6323, USA

*** Corresponding Author. Email address: smithab@sas.upenn.edu.**

Contents:

Deceased, February 2013

Spectroscopic Methods:

FTIR Spectra. FTIR spectra were collected with a Nicolet 6700 spectrometer. The spectra were corrected by solvent subtraction of d_3-TFE. After subtracting the solvent, the residual trifluoroacetic acid (TFA) absorption band from peptide synthesis counterion was also subtracted by using a measured spectra of TFA in d_3-TFE wherein the peak maximum of the TFE absorption bands were first normalized to the TFA absorption in the peptide sample. The FTIR spectrum of the unlabeled 24 residue ***S,S*-Tet-AKA** (Structure shown in Figure 1 in the main text of the article and Figure S9 in the Supplemental Information) exhibits the main amide band between 1640 cm^{-1} and 1660 cm^{-1}. Upon $^{13}C{=}^{18}O$ isotopic labeling either within the kinked region (cf. ***S,S*-Tet-AKA$_{C10*/A11*}$**, Figure S12) or away from the kinked region (cf. ***S,S*-Tet-AKA$_{A5*/A6*}$**, Figure S12), a new band is present in the spectra centered around 1595 cm^{-1} (Figure S2).

2D IR Spectroscopy. The 3.5 μJ mid IR pulse is then split by a 45 degree CaF_2 wedged window such that 5% of front surface reflection goes to the probe beam and 90% transmission is used for pump beam. The Mid IR pump beam is transmitted through either a homebuilt acoustic-optic modulated pulse shaper or a Mach-Zehnder interferometer to create a narrowband pulse or a pair of pulses, respectively, for the 2D IR measurements. The design of the acoustic-optic modulated pulse shaper is a similar to previously described experimental apparatus (1-3), with the exception that an X5-TX D/A converter module (Innovative Photonic Solutions) is used as an arbitrary wave generator for narrow band shaping. The Mid IR pump and probe beams are focused on the sample by the parabolic focusing mirror with 200 and 160 micron spot sizes, respectively, and overlapped with the optical pump beam. A pump bandwidth of 7 cm^{-1} is used for the narrow band pump broadband probe 2D IR. In the case of generating the pair of pump pulses in the pump probe geometry, a Mach-Zehnder interferometer was used to split the pulse accordingly. The Mid IR pump and probe beams are focused on the sample by the parabolic focusing mirror with 200 and 160 micron spot sizes, respectively, and overlapped with the optical pump beam. The 2D IR probe pulses were preceded by a 700 fs pump pulse (~300 μm spot size) at 355 nm with 7 μJ of energy to generate the photorelease of the tetrazine constraint. The IR pump beam is chopped by 500 Hz and the sample cell is rotated at 20 Hz to avoid the overlap between pumped and unpumped spots in the experiment. The heterodyned photon echo signal is directed to a monochromator equipped with a 64 element mercury cadmium telluride array detector (InfraRed Associates). A schematic representation of the setup is shown in Figure S1.

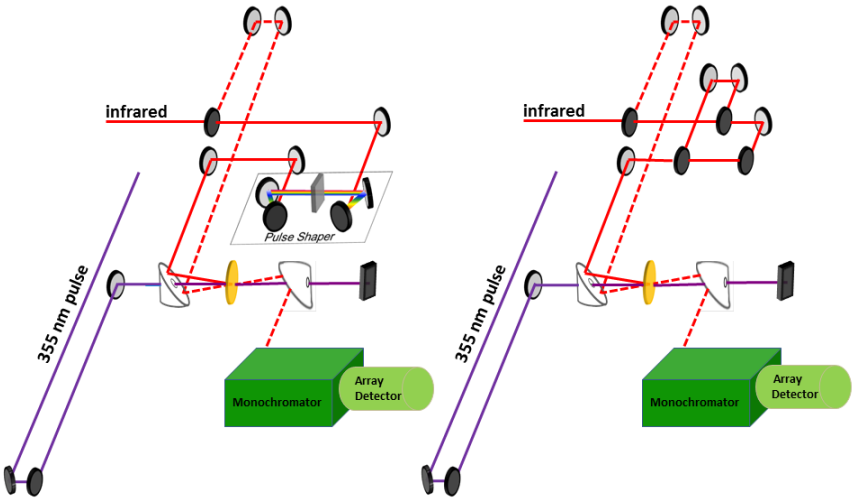

Figure S1: Optical layouts to perform UV/VIS pump 2D IR probe spectroscopy.

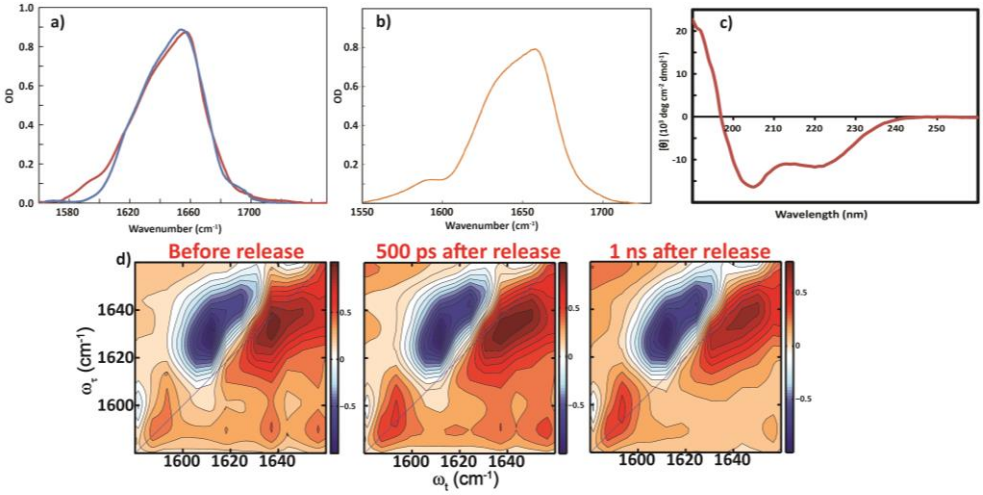

Figure S2. FTIR spectra of a) the unlabeled ***S,S*-Tet-AKA** peptide (red) and the ***S,S*-Tet-AKA$_{C10*/A11*}$** peptide with $^{13}C{=}^{18}O$ labeled pair within the kinked region at Cys10 and Ala11 (blue); b) the ***S,S*-Tet-AKA$_{A5*/A6*}$** peptide with $^{13}C{=}^{18}O$ labels at residues Ala5 and Ala6 away from the kinked region. c) The CD spectrum of the ***S,S*-Tet-AKA** tetrazine constrained peptide in d_3-TFE. d) Transient 2D IR spectra of unlabeled *S,S*-Tet-AKA in d_3-TFE before irradiation (i.e., before release), 500 ps after release, and 1 ns after release.

CAC *S,S*-Tetrazine-Linked Model Tripeptides:

The previously described tripeptide linchpins (4) corresponding to residues Cys10-Cys12 (structure **S1** in Figure S3), employed as a model peptide system, were used to provide an estimate for characterizing the behavior of this short peptide linker in the larger ***S,S*-Tet-AKA** system. The photolysis yield (~28%) to furnish the *bis*-thiocyanate peptide **S2** was measured by ns transient absorption to be slightly larger than the nonacyclic *S,S*-tetrazine oxytocin peptide we previously described (5). Although the rate of SCN formation was determined to be 66 ps for the conversion of tripeptide **S1** to **S2** (Figure S3), the rate of ring cleavage is expected to be on the order of 10s of picoseconds based on the formation of the photoproduct measured by prior experiments on dicysteine tetrazine that lacks a cyclic amide backbone (6). The 2D IR spectrum of the $^{13}C=^{18}O$-Ala peptide **S3** in CD_3OD displays a slightly narrower peak along the diagonal than that of the **S5** model peptide with both Ala11 and Cys10 residues $^{13}C=^{18}O$ labeled (Figure S4). The 2D IR diagonal traces of the $^{13}C=^{18}O$-Ala labeled **S3** peptide in CD_3OD have less than 1 cm^{-1} maximum change in spectral width, and no change in the peak position of the isotope labeled absorption band at the different optical delays (Figure S4a). The overall 2D IR spectral changes in the labeled and non-labeled tripeptide model systems upon photolysis are consistent with the picture that the labeled amide is acting as an isolated uncoupled residue. The absence of change would result from no changes in the coupling between amides. The **S5** peptide with both Ala and Cys residues $^{13}C=^{18}O$ labeled only exhibits a single transition in the 2D IR spectrum, further suggesting that the two frequency shifts of the amide are overlapping (Figure S4b). The 2D IR traces of the **S5** model tripeptide with both Ala11 and Cys10 residues $^{13}C=^{18}O$ labeled displays no significant change in the observed peak position, <0.5 cm^{-1} (Figure S4b). The spectra shape does however indicate the presence of some asymmetry that becomes more apparent immediately after photolysis of the tetrazine linker. Due to variation in the shape, the overall change in the spectral width is not systematic as a function of the different optical delays, likely due to the mixture of both hydrogen bonded and non-hydrogen bonded states in the CD_3OD solvent.

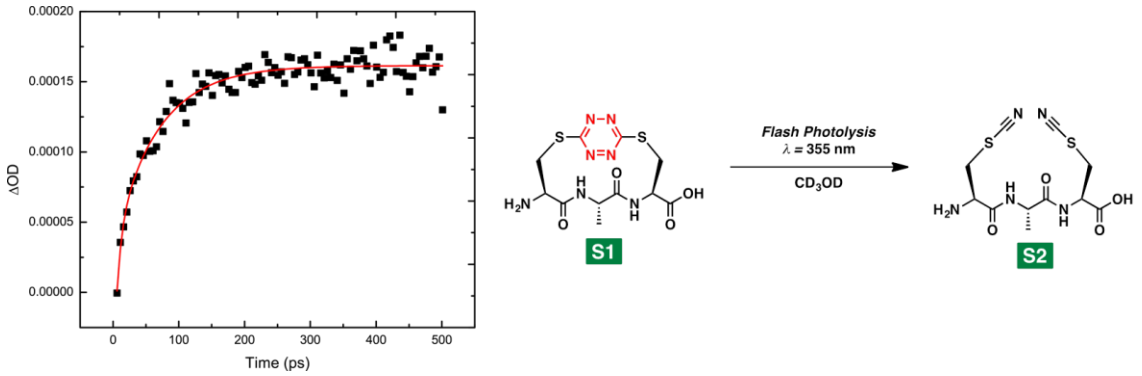

Figure S3. Picosecond transient absorption of SCN (cf. **S2**) formation following 355 nm excitation of **S1** probed at 2160cm^{-1}. The kinetic data of **S2** formation is fit to a bi-exponential rise (red) with time constants τ_1=7.6 ps and τ_2=66.2 ps.

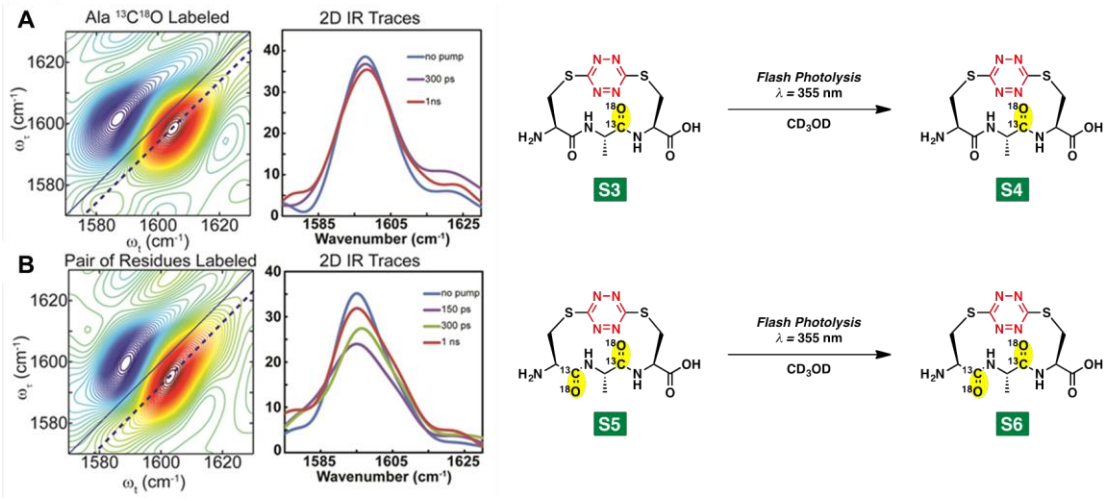

Figure S4. a.) (left) 2D IR of $^{13}C=^{18}O$-Ala labeled tripeptide **S3** prior to photolysis and (right) 2DIR traces (shown as blue dotted line in 2D spectra) of $^{13}C=^{18}O$ Ala labeled CAC peptide with no optical pump (blue), after a delay of 300 ps (purple), and 1 ns (red) demonstrating the formation of *bis*-thiocyanate tripeptide **S4**. b.) (left)2D IR of double $^{13}C=^{18}O$ labeled tripeptide **S5** prior to photolysis and (right) 2DIR traces (shown as black dotted line in 2D spectra) of with no optical pump (blue), after a delay of 150 ps (purple), 300 ps (green), and 1 ns (red) demonstrating the formation of *bis*-thiocyanate tripeptide **S6**.

It should be noted that the short model peptides are not sufficiently soluble in d_3-TFE. The NMR structure was determined for the model system (see table below for couplings) in DMSO showing that the tetrazine linkage provides a well-defined structure with an angle between the dipoles of ~144^o (4).

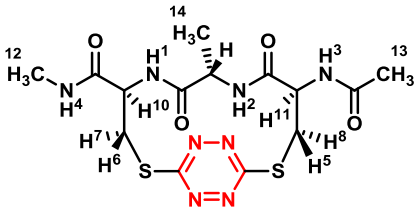

^{1}H-NMR (500 MHz, DMSO-d_6)

Proton	Shift (δ)	Splitting	Coupling Constants (Hz)		
1	8.50	d	7.5		
2	8.47	d	9.0		
3	8.03	d	7.5		
4	7.99	q	4.5		
5	4.77	dt	7.0	3.5	
6	4.66	ddd	6.5	4.5	2.0
7	4.48	dd	15.0	4.5	
8	4.41	dd	15.0	2.5	
9	4.16	dq	8.5	7.0	
10	3.44	dd	14.5	2.0	
11	3.32	dd	15.0	3.5	
12	2.63	d	4.5		
13	1.89	s			
14	1.03	d	7.0		

Table S1. H-NMR coupling parameters for CAC model peptide.

Exciton Model:

The general mathematical formulism has been described in detail previously (7, 8). Briefly, the following 5x5 Hamiltonian was used:

$$H = \begin{pmatrix} \omega_i & \beta & 0 & 0 & 0 \\ \beta & \omega_j & 0 & 0 & 0 \\ 0 & 0 & 2\omega_i - \Delta & \sqrt{2}\beta & 0 \\ 0 & 0 & \sqrt{2}\beta & \omega_i + \omega_j & \sqrt{2}\beta \\ 0 & 0 & 0 & \sqrt{2}\beta & 2\omega_j - \Delta \end{pmatrix} \qquad \textbf{[Equation 1]}$$

with the one quantum excitation of each local site represented as $|0,i\rangle$ and $|j,0\rangle$, and two quantum excitation represented as $|0,2i\rangle$, $|2j,0\rangle$ and $|j,i\rangle$. The eigenvalues and eigenvectors are calculated numerically for all possible combinations of the distribution of local mode frequencies, ω_i and ω_j. The transition dipole vectors of the local site states are at an angle, which we define as α. The dynamics of the delocalized modes are determined by their population and pure dephasing relaxation. The distribution of vibrational frequencies does not vary for the singly Ala $^{13}C=^{18}O$ labeled **S3** *S,S*-tetrazine model tripeptide for different optical pump delays, as suggested by the invariance in the experimental widths of the diagonal traces. The assumed dynamical model for the frequency-frequency correlation function has two components, a quickly decaying homogeneous dephasing, T_2^*, and a slow decay that introduces an inhomogenous width, σ. The signals are thus represented as Lorentzian functions averaged over fixed distributions of frequencies. For the computations, the nonlinear response functions are calculated on the basis of the eigenstates determined by diagonalization of the above matrix. The exciton eigenfrequencies and the transition dipole vectors are defined in terms of the pair state variables θ and ϕ, where $\tan\theta = 2|\beta|/\omega_{12}$ and $\beta = |\beta|e^{i\phi}$, with ω_{12} as the frequency gap, and β as the coupling constant. A typical response function in the frequency domain arising from Liouville pathways that involve one and two quantum excitions is described by:

$$R_1(\omega_\tau = \omega_d, \omega_t = \omega_d + c) = \frac{1}{5}\mathrm{Re}\left\langle \frac{e^{-T/T_1}\left|\vec{\mu}_{0+}\right|^4}{\left[i\left(\omega_{0+} - \omega_d\right) + \gamma_{0+}\right]\left[i\left(\omega_{0+} - \omega_d - c\right) + \gamma_{0+}\right]} \right\rangle \qquad \textbf{[Equation 2]}$$

where the angle brackets are taken over the two-site frequency distributions assumed to be uncorrelated Gaussian distributions with width σ; the frequency ω_d represent the diagonal trace displaced by c from

the center; the γ_{mn} represents the homogeneous widths, such that $2\gamma_{mn} = 1/2T_1 + 1/T_2^*(m,n;\beta,\omega_{12})$. For the least squares fitting of the diagonal traces, the center frequency of the frequency distribution, the homogenous dephasing and inhomogeneous widths, the coupling strength β, and the angle α between the dipole vectors of the uncoupled amide I modes were varied. Again, the homogeneous dephasing and inhomogeneous width did not vary significantly between delay times.

2D IR Diagonal Traces:

The 2D IR diagonal traces were obtained from the diagonal line passing through the maxima of the positive $^{13}C=^{18}O$ amide peaks of the 2D IR spectrum parallel to the $\omega_\tau = \omega_t$ main diagonal line. A linear baseline was subtracted from the isotope labeled region to eliminate the contribution from the main band. For the $^{13}C=^{18}O$ labeled 24 residue peptide ***S,S*-Tet-AKA$_{A5*/A6*}$** (i.e., with isotopic substitution distal to the kink induced by the phototrigger), the diagonal traces were fit with two gaussian bands to extract the coupling and angle between the dipoles (Figure S5). The diagonal traces of the parallel and perpendicular spectra, as a function of different optical delays, show no change in the peak separation indicating that the coupling strength does not vary (Figure S6). For the $^{13}C=^{18}O$ labeled 24 residue peptide ***S,S*-Tet-AKA$_{C10*/A11*}$** (i.e., with isotopic substitution within the kinked region) , the traces were fitted to two Lorentzian bands centered at 1580 cm^{-1} and around 1600 cm^{-1} depending on optical delay. The much weaker absorption band due to the tyrosine residue at 1580 cm^{-1}, which does not change appreciably with optical delays was subtracted from the diagonal trace spectra such that the contribution of the two isotope labels to the spectra can be directly evaluated. The systematic changes in the band around 1600cm^{-1} as a function of the different optical delays are shown in Figure S7.

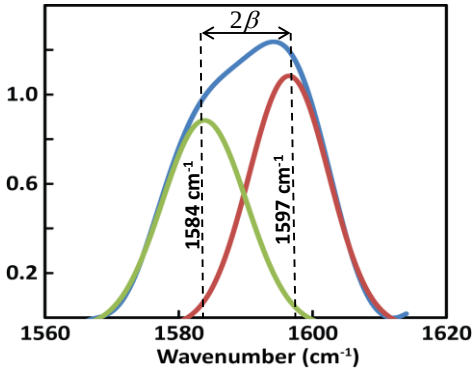

Figure S5. Diagonal trace (blue) and fit to 2 gaussians (green,red) of 2D IR spectrum of the double $^{13}C=^{18}O$ labeled ***S,S*-Tet-AKA$_{A5*/A6*}$** peptide.

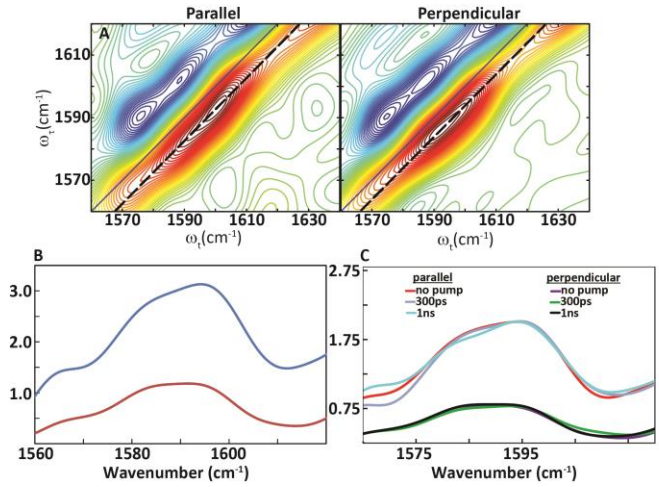

Figure S6. Spectra of 24 residue peptide with $^{13}C^{18}O$ labels at Ala5 and Ala6 in d_3-trifluoroethanol (A) Representative transient 2D-IR spectra taken with parallel (left) and perpendicular (right) infrared probe beam polarization relative to pump beam; (B) Average of 2D IR diagonal traces along the peak maximum for parallel (blue) and perpendicular (red) polarizations; (C) Normalized diagonal traces of perpendicular and parallel 2D IR spectra at different T_{opt} delays as shown of isotope labeled region of the double $^{13}C=^{18}O$ labeled peptide ***S,S*-Tet-AKA$_{A5*/A6*}$.**

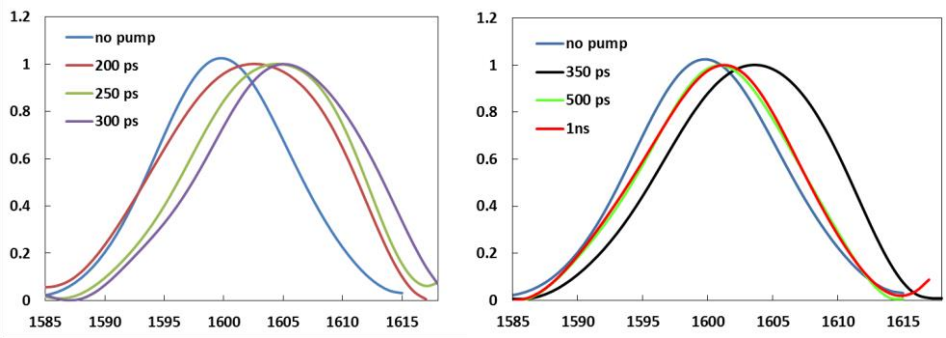

Figure S7. Diagonal traces of 2D IR spectra at different T_{opt} delay as shown of isotope labeled region of the double $^{13}C=^{18}O$ labeled peptide ***S,S*-Tet-AKA$_{C10*/A11*}$.**

MD Simulations:

The peptide of interest was immersed within a 50 Å cubic TFE box with periodic boundary conditions utilized in the three spatial dimensions to reduce edge effects. The parameters for trifluoroethanol box were adapted from the work of MacKerell (9). The Nosé-Hoover Langevin piston pressure control method was used to maintain the pressure of the cell at 1 atm during isobaric simulation runs, and in all the simulations Langevin dynamics were used to control the temperature at 298 K. The simulations were conducted with a time step of 2 fs. Nonbonded interactions were calculated at every time step and full electrostatic interactions were calculated at every two time steps. The SHAKE algorithm was employed to constrain all bonds involving the hydrogen atom to their equilibrium values (10, 11), and full electrostatic forces were calculated using the particle mesh Ewald method (12, 13).

Following an initial 1 ns equilibration run at 298 K and 1 atm in the NPT ensemble, a productive run at 298 K in the NVT ensemble was carried out.

To model the changes in the data, both equilibrium and non-equilibrium molecular dynamics (MD) simulations were performed using the CHARMM22 force fields. To obtain the equilibrium distribution, a helical AKA(A10C/A12C) peptide and a harmonically constrained AKA(A10C/A12C) peptide to model the ***S,S*-Tet-AKA** peptide were placed in an equilibrated TFE box. The constrained AKA(A10C/A12C) peptide was constructed with the sulfur-sulfur distance between the two Cys residues and the distances between the S atom of each Cys with the hydrogen of the other Cys side chain harmonically constrained with k=10 kcal/(mol $Å^2$) in place of the tetrazine due to the lack of force field parameterization. After energy minimization of the complete peptide and explicit solvent system, a production run was performed to obtain a distribution of structures for the helical and harmonically constrained peptides over 4 ns. After acquiring the equilibrium distribution of the constrained peptides, the constraints were then released and the non-equilibrium simulations were run to obtain structural changes. From the structural distribution, a distribution of frequencies was obtained by using an empirical amide I vibrational map developed by Skinner and coworkers (14). In addition, the coupling between nearest neighbor amides were determined by using well known coupling maps derived from calculations that characterize the coupling as a function of phi,psi angles of a peptide backbone (15, 16). By combining the uncoupled frequencies, the coupling constants from the phi,psi maps, and the angle between dipoles, the 2D IR spectra could be simulated using an exciton model over the frequency distribution computed from the MD simulation. The autocorrelation decay was determined from the RMSD of the nonequilibrium trajectories upon release of the constraint with respect to the average helical equilibrium structure. The time constant of the correlation decay was determined from an exponential fit to be 148 ps (Figure S8). The full 10 ns trajectory is shown for both the decrease in angle between the dipoles and the increase in the coupling between the dipoles (Figure S8). It should be noted that no significant changes in the distribution were observed after 500 ps.

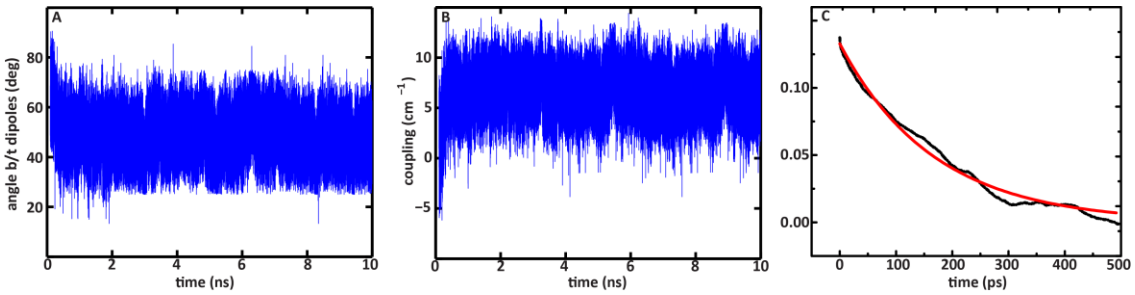

Figure S8. A) Decay of the angle between dipoles and B) increase in the coupling between dipoles from mean nonequilibrium MD trajectory for duration of 10 ns. C) Autocorrelation decay of RMSD of nonequilibrium trajectory upon release of constraint with respect to average helical equilibrium reference structure.

Peptide Synthesis:

The full experimental details of the three fragment coupling approach to construct the 24 residue ***S,S*-Tet-AKA** peptide will be described in a separate manuscript. Briefly, solid-phase peptide synthesis (SPPS) was carried out in peptide synthesis reaction vessels (25 or 50 mL) with a coarse fritted glass support and Teflon stopcocks. The reaction vessels had 14/20 ground glass joints that allowed the resin to be kept under a nitrogen atmosphere. Analytical high-performance liquid chromatography-mass spectrometry (HPLC-MS) analyses were conducted with an instrument comprised of a Waters 2767 sample manager, a Waters 2525 binary gradient HPLC pump that are connected to a diode array detector, and a Waters Micromass ZQ mass spectrometer with electro-spray ionization. The HPLC-MS samples were analyzed as solutions in water or acetonitrile (0.15–0.20 mg/mL concentration). The HPLC-MS chromatography was carried out on an Atlantis–C18 column (4.6 ×50 mm; 5 µm; Waters Corporation) with linear gradients of 0.05% formic acid in acetonitrile and 0.05% formic acid in ultra pure water. Preparative-scale reverse-phase high-preformance liquid chromatography (HPLC) was conducted with a Gilson system comprised of a 215 liquid handler/injector unit fitted with binary Gilson 333/334 HPLC pumps and a Model 156 UV/vis dual wavelength detector. The chromatograms were processed with the Trilution software provided by the manufacturer. The peptide fragments and the final ***S,S*-Tet-AKA** peptide were purified with a Waters XBridge Prep BEH 130 C18 5µm OBD 19 × 100mm column and were >95% pure. The mobile phase for HPLC-MS analysis and preparative scale HPLC purification of peptide fragments **S7**-**S9** (Figure S9) consisted of acetonitrile (HPLC grade) containing 0.05% formic acid and ultrapure water containing 0.05% formic acid. The mobile phase for the preparative scale reverse-phase HPLC purification of the final synthetic peptides (i.e., ***S,S*-Tet-AKA**, ***S,S*-Tet-AKA$_{A5*/A6*}$**, and ***S,S*-Tet-AKA$_{C10*/A11*}$,** Figure S12) peptide consisted of acetonitrile (HPLC grade) containing 0.05% trifluoroacetic acid and ultrapure water containing 0.05% trifluoroacetic acid. High-resolution mass spectra were obtained with a Waters LC-TOF mass spectrometer (model LCT-XE Premier) using electrospray ionization. Matrix-assisted laser desorption ionization (MALDI) mass spectra were collected with a Bruker Ultraflex III MALDI-TOF-TOF employing α-cyano-4-hydroxycinnamic acid as the matrix. The high-resolution and MALDI mass spectra were obtained in the Mass Spectrometry Facility within the Department of Chemistry at the University of Pennsylvania.

The *N*-terminal peptide fragment **S8** (Figure S9) was prepared through standard SPPS on the 2-chloro trityl resin (Novabiochem). The tripeptide *S,S*-tetrazine linchpin **S7** and ^{13}C and $^{13}C{=}^{18}O$ isotopically edited tripeptides were prepared following previously described procedures (4). The *C*-terminal peptide fragment **S9** was constructed through SPPS employing the *N*-methyl indole aminomethyl resin (Novabiochem). The side-chain protected peptide fragments **S7**-**S9** were purified by preparative scale HPLC. Next, a four step protocol was utilized to construct ***S,S*-Tet-AKA**. Step 1: Amide bond

formation in solution mediated by HBTU, followed by preparative HPLC purification. Step 2: Boc protecting group removal by treatment with TFA/MeCN (1:3 v/v). Step 3: Amide bond formation in solution mediated by HBTU to complete construction of the full amide backbone. Step 4: Cbz protecting group removal from the Lys residue side chains, followed by preparative HPLC purification. Following lyopholyzation, the ***S,S*-Tet-AKA** peptide was obtained as a pale orange amorphous powder. Analytical HPLC-MS (5% to 60% MeCN in H_2O over 7 min): HRMS (ES) *m/z* 2213.1260 $[(M+H)^+$; calcd for $C_{93}H_{154}N_{33}O_{26}S_2$: 2213.1184]; MALDI-TOF *m/z* 2213.598 $[(M+H)^+$; calcd for $C_{93}H_{154}N_{33}O_{26}S_2$: 2213.1184]. (Figures S11-S12)

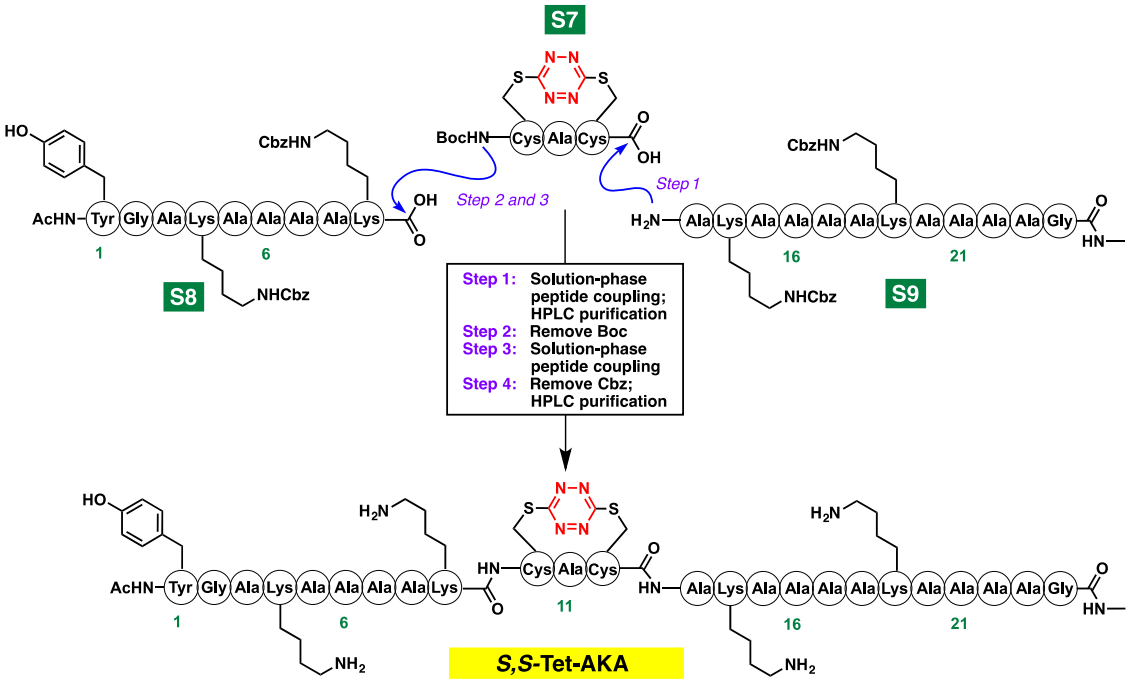

Figure S9. The synthetic approach to the ***S,S*-Tet-AKA** peptide.

Isotopically edited peptides containing $^{13}C/^{18}O$ amide 2D-IR vibrational labels were prepared by substituting the appropriate $^{13}C/^{18}O_2$ labeled amino acids at the desired positions (Figure S10). We have previously described both the synthesis of the Cys10*/Ala11* labeled tripeptide linchpin (4). The $^{13}C=^{18}O$ labeled Fmoc-Ala-$^{13}C^{18}O_2H$ was prepared according to known procedures (17). Following the procedures described above, we successfully constructed ***S,S*-Tet-AKA$_{C10*/A11*}$** and ***S,S*-Tet-AKA$_{A5*/A6*}$**. ***S,S*-Tet-AKA$_{C10*/A11*}$**: HRMS (ES) *m/z* 2219.1348 $[(M+H)^+$; calcd for $^{12}C_{91}{}^{13}C_2H_{154}N_{33}{}^{16}O_{24}{}^{18}O_2S_2$: 2219.1336]; MALDI-TOF *m/z* 2219.522 $[(M+H)^+$; calcd for $^{12}C_{91}{}^{13}C_2H_{154}N_{33}{}^{16}O_{24}{}^{18}O_2S_2$: 2219.1336] (Figures S13-S14). ***S,S*-Tet-AKA$_{A5*/A6*}$**: HRMS (ES) *m/z* 2219.1357 $[(M+H)^+$; calcd for $^{12}C_{91}{}^{13}C_2H_{154}N_{33}{}^{16}O_{24}{}^{18}O_2S_2$: 2219.1336]; MALDI-TOF *m/z* 2219.781 $[(M+H)^+$; calcd for $^{12}C_{91}{}^{13}C_2H_{154}N_{33}{}^{16}O_{24}{}^{18}O_2S_2$: 2219.1336] (Figures S15-S16).

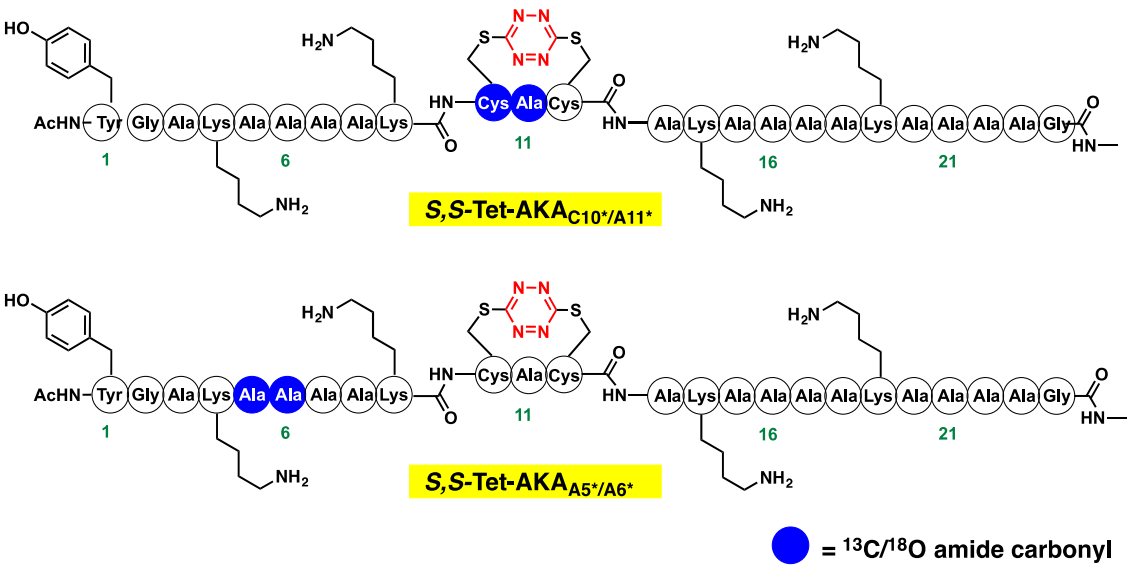

Figure S10. The positions of $^{13}C/^{18}O$ labeled amides in the ***S,S*-Tet-AKA$_{C10*/A11*}$** and ***S,S*-Tet-AKA$_{A5*/A6*}$**.

Peptide Sample Preparation:

The ***S,S*-Tet-AKA**, ***S,S*-Tet-AKA$_{C10*/A11*}$** and ***S,S*-Tet-AKA$_{A5*/A6*}$** peptides, as ~3-5 mM solutions in CD_3OD (Fisher) or d_3-trifluoroethanol (Sigma-Aldrich), were used for transient 2D IR experiments. To determine an approximate structure for the kinked region of the ***S,S*-Tet-AKA** peptide, the solution structure of **S1** (Figure S3) was characterized by NMR spectroscopy (4) to yield a structure with an angle of 144^o between the two internal amide groups deviating from the angle expected for a standard helix ranging from 50-70 degrees (*vide supra*). Upon photolysis (λ = 355nm), the tetrazine ring cleaves on a timescale of tens of picoseconds to ultimately form two SCN groups with a photolysis yield of >25% (5, 6). The peptide linchpin (cf. **S1**) was incorporated into a 24 residue alanine-based helical peptides, such that residues 10 and 12 were linked by the tetrazine trigger (Figure 1 and Figure S9). All experiments on the ***S,S*-Tet-AKA**, ***S,S*-Tet-AKA$_{C10*/A11*}$** and ***S,S*-Tet-AKA$_{A5*/A6*}$** peptides were performed in d_3-trifluoroethanol (d_3-TFE) to increase solubility and overall helical propensity (18). A constrained molecular dynamics simulation suggests the peptide adopts a helical structure with a kink around the linchpin. The remaining helicity (>50%), very close to the native structure, was confirmed using circular dichroism (from the ellipicity at 222nm) with a slight increase in helicity upon photolysis (Figure S2c). The optical density at the excitation wavelength of the samples ranges from 0.09-0.12 in a 400 μm path length CaF_2 cell. The excitation wavelength was 355 nm. Based on the fraction of the excited molecules (>70%), it is expected that the shape of spectra is primarily influenced only by photolyzed sample at the

different time delays. All FTIR spectra were taken on a Nicolet 6700 FTIR spectrometer. The absorption spectra were collected on a Perkin–Elmer Lambda 25 UV-Vis spectrometer (Fremont, CA, USA).

References:

1. Shim SH, Strasfeld DB, Fulmer EC, & Zanni MT (2006) Femtosecond pulse shaping directly in the mid-IR using acousto-optic modulation. *Opt. Lett.* 31(6):838-840.
2. Shim SH, Strasfeld DB, Ling YL, & Zanni MT (2007) Automated 2D IR spectroscopy using a mid-IR pulse shaper and application of this technology to the human islet amyloid polypeptide. *Proc. Natl. Acad. Sci. U.S.A* 104(36):14197-14202.
3. Shim SH & Zanni MT (2009) How to turn your pump-probe instrument into a multidimensional spectrometer: 2D IR and Vis spectroscopies via pulse shaping. *PCCP* 11(5):748-761.
4. Abdo M, *et al.* (2012) Design, Synthesis, and Photochemical Validation of Peptide Linchpins Containing the S,S-Tetrazine Phototrigger. *Org. Lett.* 14(13):3518-3521.
5. Tucker MJ, *et al.* (2010) Tetrazine Phototriggers: Probes for Peptide Dynamics. *Angew. Chem. Int. Ed.* 49(21):3612-3616.
6. Tucker MJ, *et al.* (2012) Di-cysteine S,S-tetrazine: A potential ultra-fast photochemical trigger to explore the early events of peptide/protein folding. *J. Photochem. Photobiol., A* 234:156-163.
7. Remorino A & Hochstrasser RM (2012) Three-dimensional structures by two-dimensional vibrational spectroscopy. *Acc. Chem. Res.* 45(11):1896-1905.
8. Remorino A, Korendovych IV, Wu Y, DeGrado WF, & Hochstrasser RM (2011) Residue-specific vibrational echoes yield 3D structures of a transmembrane helix dimer. *Science* 332(6034):1206-1209.
9. Chen IJ, Yin DX, & MacKerell AD (2002) Combined ab initio/empirical approach for optimization of Lennard-Jones parameters for polar-neutral compounds. *J. Comput. Chem.* 23(2):199-213.
10. Ryckaert JP, Ciccotti G, & Berendson HJC (1977) Numerical integration of the cartesian equations of motion of a system with constraints: molecular dynamics of *n*-alkanes. *J. Comput. Phys.* 23(3):327-341.
11. Andersen HC (1983) Rattle: A "velocity" version of the shake algorithm for molecular dynamics calculations. *J. Comput. Phys.* 52(1):24-34.
12. Darden T, York D, & Pederson L (1993) Particle mesh Ewald: An *N*-log(*N*) method for Ewald sums in large systems. *J. Chem. Phys.* 98(12):10089-10092.
13. Essmann U, *et al.* (1995) A smooth particle mesh Ewald method. *J. Chem. Phys.* 103(19):8577-8593.
14. Wang L, Middleton CT, Zanni MT, & Skinner JL (2011) Development and Validation of Transferable Amide I Vibrational Frequency Maps for Peptides. *J. Phys. Chem. B* 115(13):3713-3724.
15. Torii H & Tasumi M (1998) Ab initio molecular orbital study of the amide I vibrational interactions between the peptide groups in di- and tripeptides and considerations on the conformation of the extended helix. *J. Raman Spectrosc.* 29(1):81-86.
16. Jansen TlC, Dijkstra AG, Watson TM, Hirst JD, & Knoester J (2006) Modeling the amide I bands of small peptides. *J. Chem. Phys.* 125(4).
17. Fang C, *et al.* (2004) Two-dimensional infrared spectroscopy of isotopomers of an alanine rich alpha-helix. *J. Phys. Chem. B* 108(29):10415-10427.
18. Luo PZ & Baldwin RL (1997) Mechanism of helix induction by trifluoroethanol: A framework for extrapolating the helix-forming properties of peptides from trifluoroethanol/water mixtures back to water. *Biochemistry* 36(27):8413-8421.

Peptide Sample Characterization: LC-MS and MALDI-TOF MS

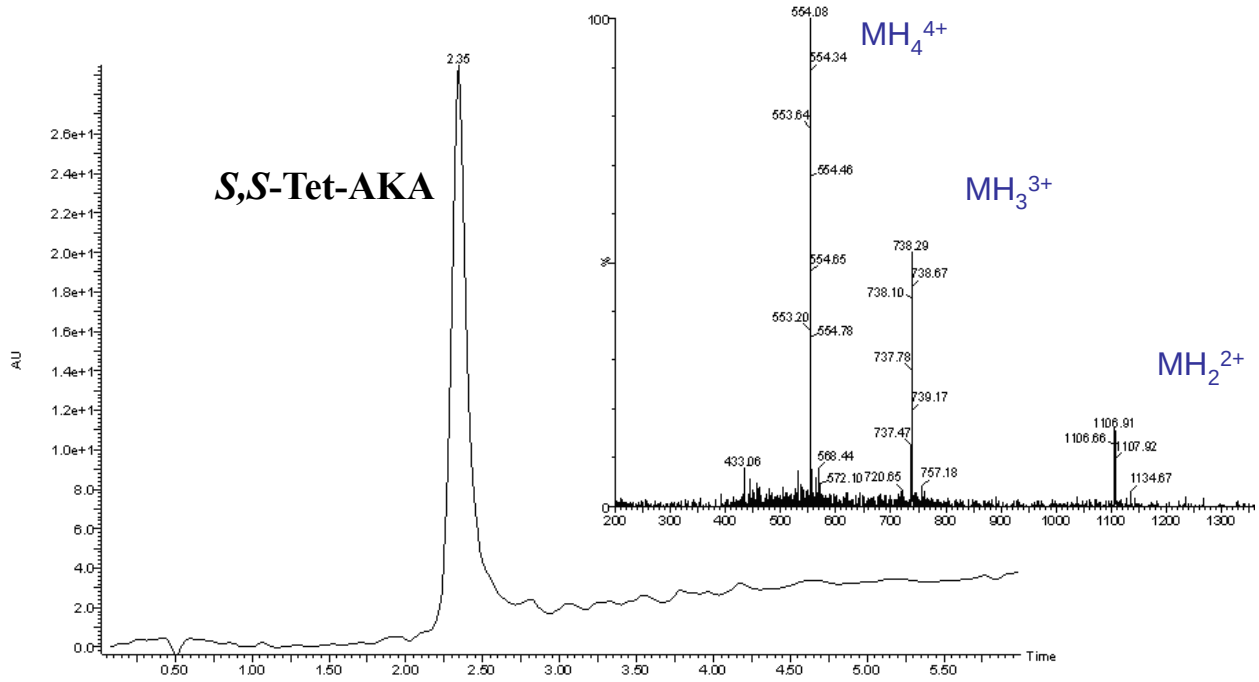

Figure S11. The HPLC-MS analysis of the purified ***S,S*-Tet-AKA** peptide.

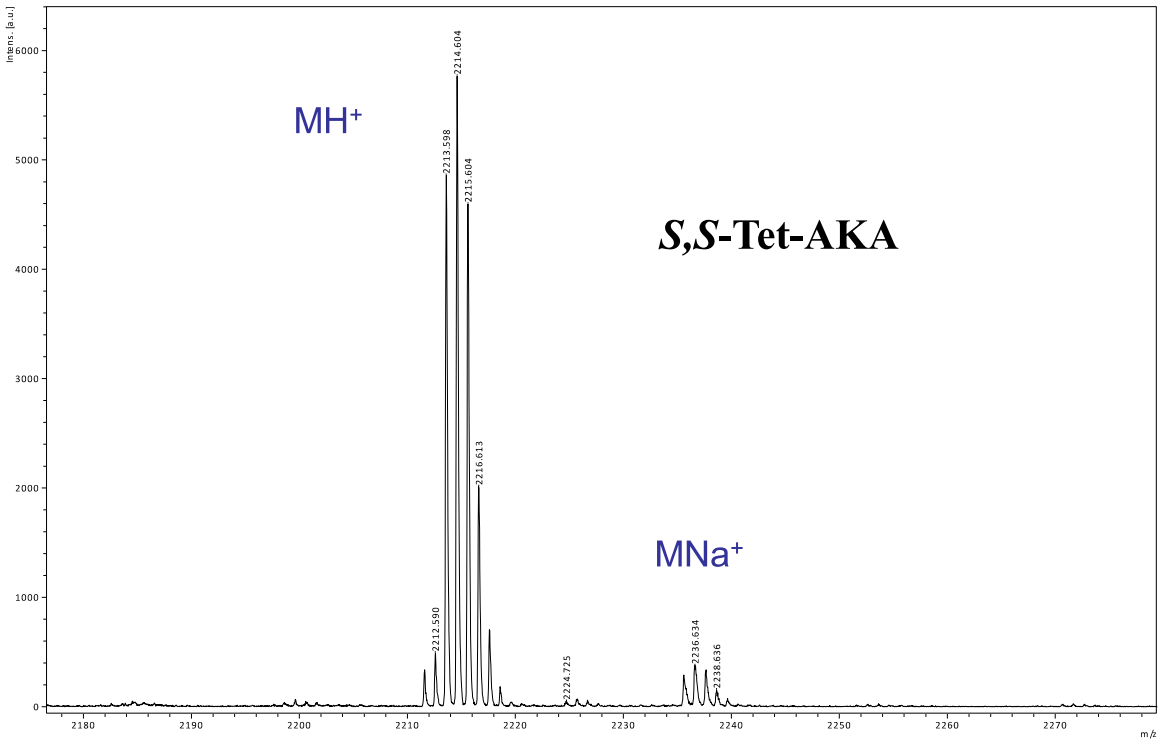

Figure S12. The high-resolution MALDI-TOF MS of the ***S,S*-Tet-AKA** peptide.

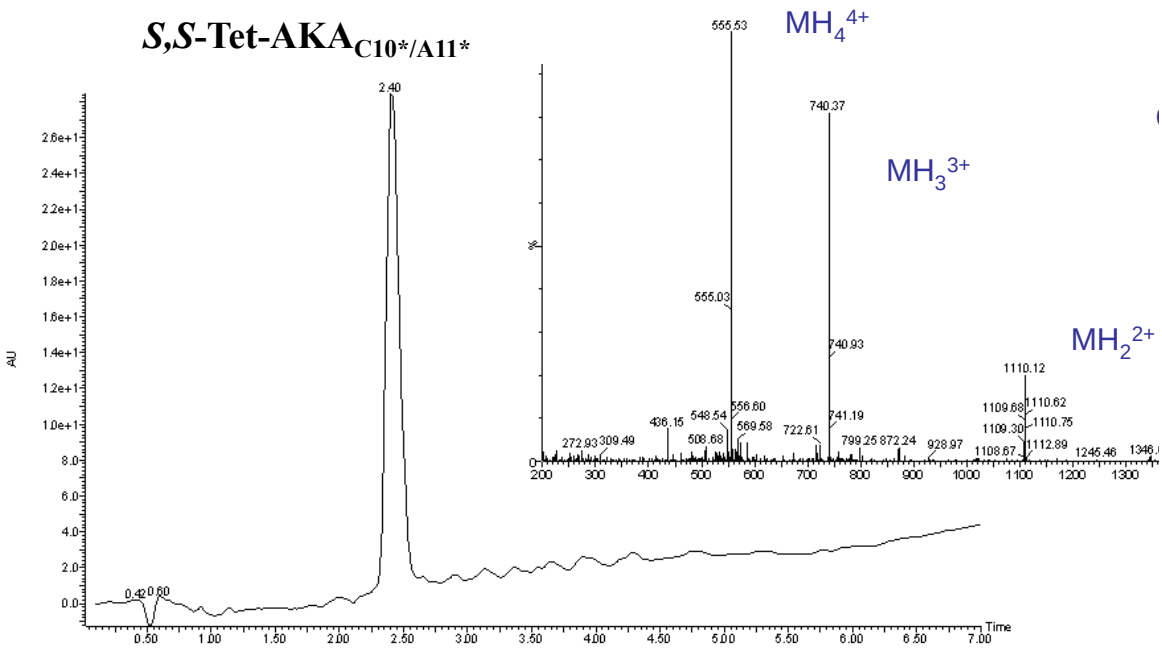

Figure S13. The HPLC-MS analysis of the purified ***S,S*-Tet-AKA$_{C10*/A11*}$** peptide.

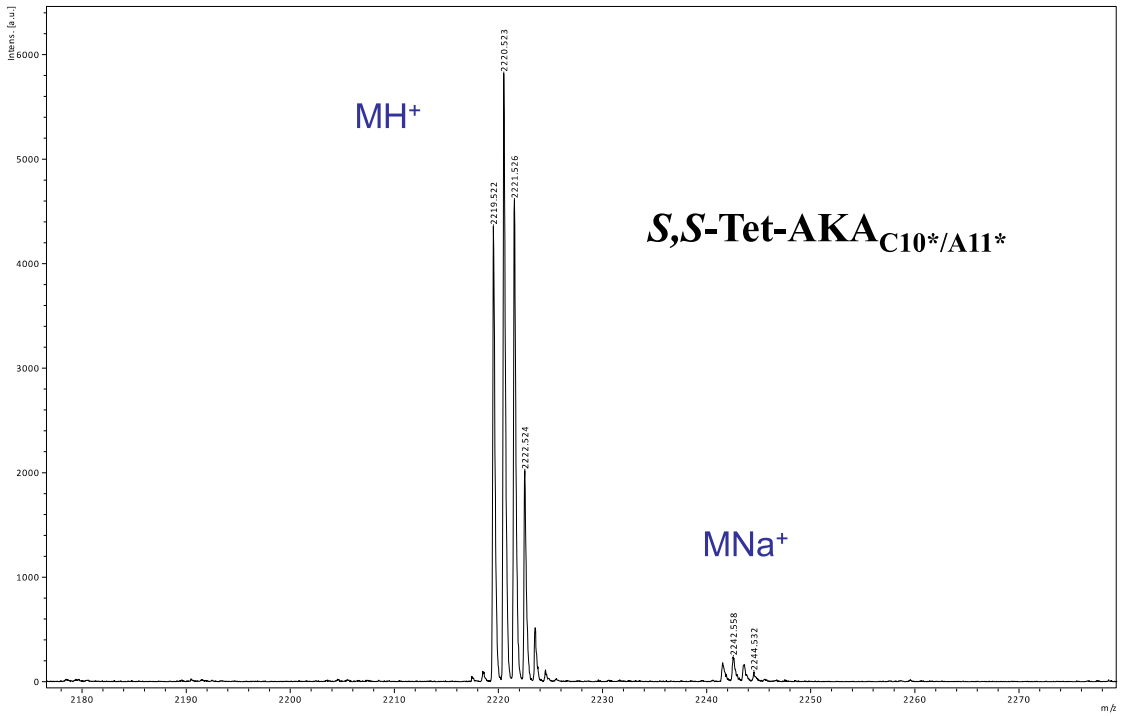

Figure S14. The high-resolution MALDI-TOF MS of the ***S,S*-Tet-AKA$_{C10*/A11*}$** peptide.

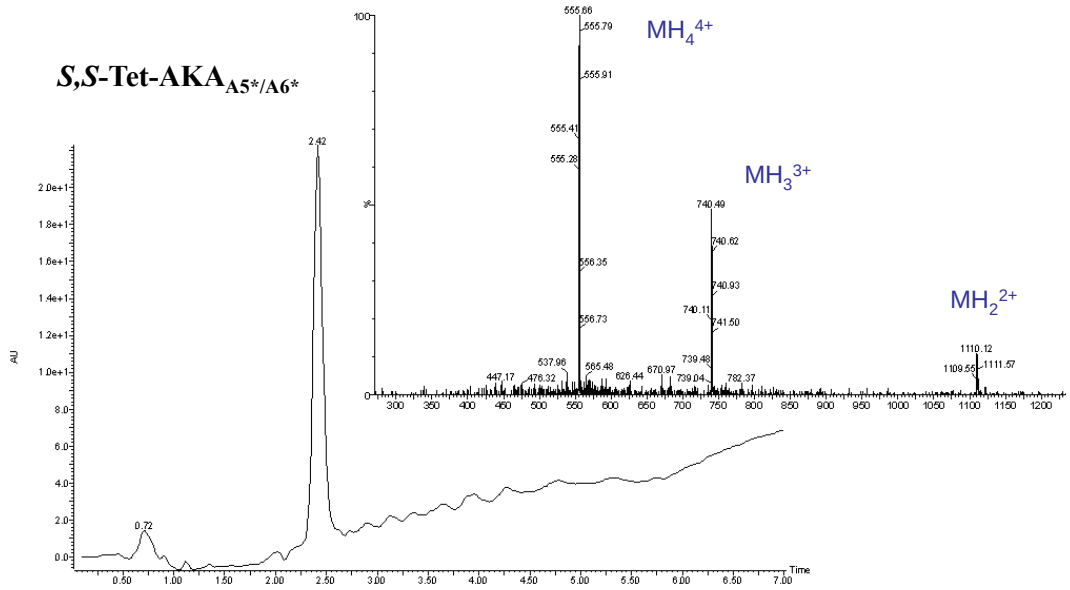

Figure S15. The HPLC-MS analysis of the purified ***S,S*-Tet-AKA$_{A5*/A6*}$** peptide.

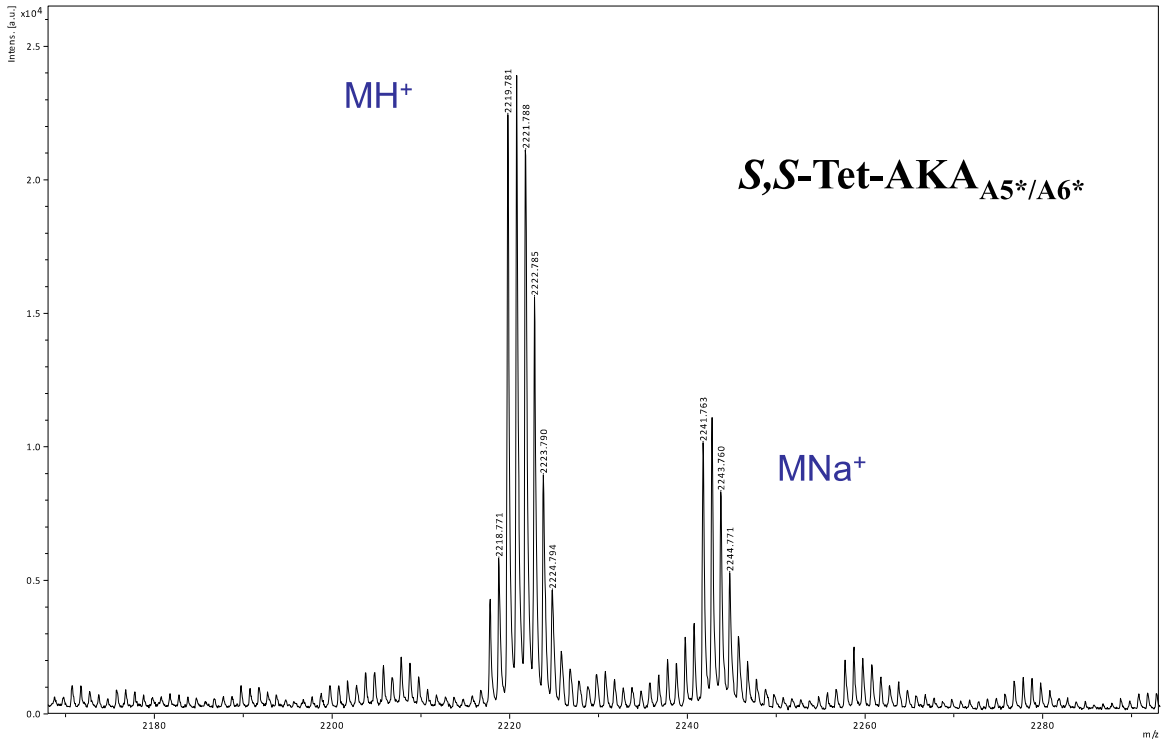

Figure S16. The high-resolution MALDI-TOF MS of the ***S,S*-Tet-AKA$_{A5*/A6*}$** peptide.